Journal of Materials Processing Tech. 309 (2022) 117738

Contents lists available at ScienceDirect

Journal of Materials Processing Tech.

journal homepage: www.elsevier.com/locate/jmatprotec

Pore formation and melt pool analysis of laser welded Al-Cu joints using synchrotron radiation

S. Hollatz [a,*], M. Hummel [b], A. Olowinsky [a], A. Gillner [a,b], F. Beckmann [c], J. Moosmann [c]

[a] Fraunhofer Institute for Laser Technology ILT, Steinbachstr. 15, 52074 Aachen, Germany
[b] Chair for Laser Technology LLT, RWTH Aachen University, Steinbachstr. 15, 52074 Aachen, Germany
[c] Institute of Materials Physics, Helmholtz-Zentrum HEREON, Max-Planck-Str. 1, 21502 Geesthacht, Germany

ARTICLE INFO

Associate Editor: Dr Jian Cao

Keywords:
Laser welding
Synchrotron
Aluminium
Copper
Melt pool dynamics
Pore formation

ABSTRACT

Known as challenging material combination, the welding of aluminium and copper, both with strongly different thermophysical properties, causes joining failures such as pores, cracks or intermetallic phases in the solidified welding area. To investigate the mixing of the materials and the occurrence of pores, the laser welding process is observed with synchrotron radiation which visualizes the phase boundaries between solid, liquid and gaseous material phases. This allows the visualization of pore formation and density differences of the materials inside the melt pool. In this investigation, pore formation in front and bottom of the keyhole is observed. The movement of the bubbles in the melt pool can be tracked until solidification at the material transition. Regarding the intermixing of the materials, the high-speed images show a fluctuating copper flow towards the keyhole and a material mixing over the entire aluminium melt pool depth. By understanding the mechanisms, compensatory measures for an improved process can be developed to enable the usability of aluminium and copper connections, for example in electromobility applications.

1. Introduction

To reduce the CO_2-emission, the international automotive industry is developing an increasing number of battery electric vehicles. Increasing electrification and the development of battery storage systems require a variety of high-quality electrical connections. Due to the aluminium and copper electrodes of the Li-ion cells, dissimilar material joints must be created for the connection of battery cells to a battery storage system (Lee et al., 2010). The challenge in welding aluminium and copper is the formation of pores, intermetallic phases and cracks which increase the electrical resistance of the joint (Schmidt et al., 2012).

Commonly used manufacturing techniques in battery applications are resistance spot welding, ultrasonic welding, and laser beam welding (Das et al., 2018). Talking about aluminium and copper, the high thermal and electrical conductivity is challenging for the cheap and well-known resistance welding process. Ultrasonic welding is limited due to material thickness, high demand on the surface condition and induced vibration stress (Brand et al., 2015). The high level of automation, process speed and mechanical contactlessness make the laser welding process a promising process for this application (Das et al., 2018).

In laser beam welding, a differentiation is made between heat conduction welding and deep penetration welding. Deep penetration welding is based on evaporation of material due to absorption of laser radiation. When a material-dependent intensity threshold is exceeded, a vapor capillary (keyhole) is formed. The resulting keyhole is moved through the workpiece by laser movement and leads, compared to heat conduction welding, to narrow and deep weld seams. During a deep penetration welding process, different melt pool flows occur. The displacement of material due to the relative movement of the vapor capillary and the workpiece, results in a backward flow of material around the capillary. At the same time, the metal vapor escaping from the capillary generates an acceleration of the adjacent melt in the direction of the capillary opening. A third effect is based on the temperature dependence of the surface tension of the melt. This moves the near-surface melt from hot areas close to the capillary towards the cooler edge of the melt pool (Hügel and Graf, 2009).

To increase the process stability and to adjust the weld seam geometry, a spatial power modulation (a superposition of the feed rate with an oscillation movement) is used (Schmitt, 2012).

There are several investigations on the mixing of aluminium and copper during laser welding. Balu et al. (2011) have investigated

* Corresponding author.
E-mail address: soeren.hollatz@ilt.fraunhofer.de (S. Hollatz).

https://doi.org/10.1016/j.jmatprotec.2022.117738
Received 7 April 2022; Received in revised form 20 July 2022; Accepted 27 July 2022
Available online 29 July 2022

different welding arrangements, for example Cu on top of Al or vice versa. The weld seam geometry in cross section has been analysed, resulting in a wider weld seam on aluminium side due to the lower thermal conductivity and melting point. Hardness measurements suggest the occurrence of intermetallic phases (Balu et al., 2011). Further research is dealing with the influence of the laser parameters and the usage of beam oscillation on mechanical and electrical properties of the dissimilar joint. Kraetzsch et al. (2011) could achieve crack free welds by using a high frequency beam oscillation. Dimatteo et al. (2019) have discovered increase mechanical properties by decreasing the penetration depth in lap joints. An investigation of the intermetallic phases relative to the percentage of aluminium in the melt pool has been conducted by Bantel (2018). The EDX analysis leads to the conclusion, that a higher percentage of aluminium in the melt pool reduces the occurrence of critical intermetallic phases and improves the mechanical properties of the lap joint. Measurements of the electrical resistance of each intermetallic phase were performed by Rabkin et al. (1970). Compared to the base material, the resistance increases for all intermetallic phases. For the theta phase, there is an increase by a factor of almost six.

A major influence on intermetallic phase and crack formation is the mixing of the materials. This in turn is dependent on the melt pool dynamics, caused by the vapor capillary and the weld depth as a measure for the material ratio in the melt (considering a lap joint). Using an x-ray phase contrast method, the keyhole and solid-liquid interface can be observed during laser welding. Miyagi et al. (2017) have identified instabilities at the keyhole bottom as a reason for porosity formation in aluminium using x-ray analysis. They have observed pores, formed at the keyhole bottom, moving towards the surface, and being trapped at the solid-liquid interface in the back of the melt pool. Keyhole instabilities are also identified by Fetzer et al. (2018) as a main driving force for the formation of pores in aluminium welding with x-ray analysis. As a different method to identify pore formation during the welding process, a butt joint configuration with glass and stainless steel can be used. The laser beam is focused on the steel close to the edge. With this setup, Xu et al. (2018) have observed a keyhole fluctuation and collapse, resulting in bubble formation.

Cunningham et al. (2019) suggest a relationship between the appearance of pores and the aspect ratio of the keyhole depending on the ratio of laser power and feed rate. By using x-ray synchrotron radiation, they could observe keyhole instabilities and bubble formation while welding titanium alloys for application in laser powder bed fusion. A detailed visualisation of a keyhole collapse, bubble formation and an analysis of the bubble size including a pore splitting are published by Zhao et al. (2020). They assume that acoustic waves as well as a fluctuating keyhole can drag away the bubbles from the keyhole to the solidification area resulting in pore trapping. The acoustic waves occur after the bubble has detached from the keyhole, as it contracts into a sphere.

Welding aluminium and copper, x-ray analysis additionally enables the visibility of the material mixing due to different density. Leitz (2016) derives melt pool flows from x-ray videography and metallographic analysis for an aluminium and copper welding process. The results of an x-ray analysis for aluminium and copper welds are also addressed in this paper. In contrast to the existing investigations, synchrotron radiation is used in this work with the goal of improving the quality and contrast of the images. The pore formation and movement as well as the melt pool dynamics are in the focus of the discussions. To analyse in detail the formation mechanisms in dissimilar material welding configurations, aluminium and copper are welded in overlap configuration with two different infrared laser beam sources of different laser focus diameters (see Table 2).

2. Experimental setup for laser welding of aluminium and copper with synchrotron radiation

The experimental setup for this investigation is based on the usage of the high energy beamline P07 (EH4) of Petra 3 at Deutsches Elektronen Synchrotron DESY in Hamburg, Germany (Schell et al., 2013). To observe the welding process, the x-ray radiation is transmitting the metal probe and is detected by a $CdWO_4$ (Cadmiumwolframat) scintillator. Using a Photron Fastcam SA5, the intrinsic glow of the scintillator screen stimulated by the X-rays is recorded. The pictures were taken with 1024 × 768 pixels with a frame rate of 1 kHz and 1 ms exposure time. The synchrotron setup and parameters are shown in Table 1.

The setup for the laser welding includes a high-speed axis to apply the feed rate, a scanning system with optics and the laser beam sources. For the investigations two laser beam sources with different spot diameters are used. A schematic of the setup is shown in Fig. 1.

More information about the set up can be found in Wagner et al. (2021).

2.1. Laser beam characteristics for experimental investigation

To compare the influence of different spot diameters on the shape of the keyhole, a single-mode fibre laser and a multi-mode disk laser are used. The characteristics of the laser beam sources are shown in Table 2.

The used laser beams sources differ by a factor of about three in the resulting focal diameter. The laser beams are guided through a scanner system and f-theta optics to the workpiece surface. The beam position is fixed, while the workpiece is moving with the feed rate. The stationary laser beam is necessary to have a fixed position for the x-ray beam. The scanner system is used to initially arrange the laser beam and to apply a circular spatial power modulation. Thus, the following results differ in focal diameter, laser power, feed rate as well as amplitude (radius) and frequency of the spatial power modulation.

2.2. Material preparation for X-ray analysis

The workpieces for the investigation are based on 3 mm thick metal sheets which are irradiated by the x-rays. The material samples are 30 mm in height and 100 mm in length. For the investigation of the dissimilar lap joints, sheets with 0.5 mm in height are welded to the top of the base metal sheets. As top layers Al99.5 and Cu-ETP are used with CuSn6 and Al99.5 as base materials. The properties of the used materials are shown in Table 3.

2.3. Process observation with synchrotron radiation

The captured grey scale images are post processed using shading technology and Kalman filtering (Kalman, 1960) to improve the visibility of the phase boundaries and contrasts. Images are recorded with a frame rate of 1000 images per second. In Fig. 2 individual frames of three different welding processes are compared as an example. On the left, a bead on plate welding of aluminium is shown as a reference. The phase boundary of the melt pool and the keyhole are visible, while the position of the laser beam is indicated. Using aluminium and copper connections, the higher optical density of the copper material prevents visibility inside the copper.

However, in the aluminium material of the dissimilar joints the keyhole, partially the phase boundary of the melt pool, pores and darker veils in the melt pool can be identified. These darker areas aren't visible

Table 1
Characteristics and parameters of the synchrotron (Hummel et al., 2021).

Parameter	Unit	P07 Petra 3
Operation Mode	[-]	Low Beta
Photon energy	[keV]	37,7
Beam area	[mm2]	2 × 2
Scintillator material	[-]	CdWO4
Scintillator size	[mm2]	11 × 11
Scintillator thickness	[μm]	300
Distance scintillator – material sample	[mm]	800

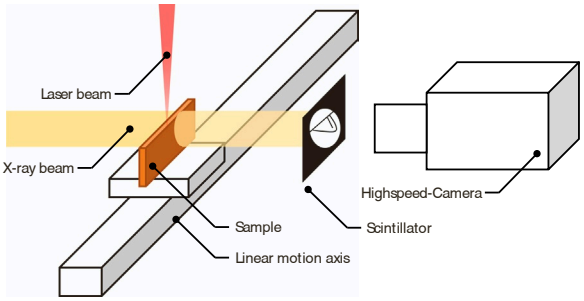

Fig. 1. Schematic of the used synchrotron setup (Wagner et al., 2021).

Table 2
Characteristics of the used laser beam sources.

Parameter	Unit	YLR-2000WC	TruDisk 5000
Wavelength	[nm]	1070	1030
Laser power	[W]	2000	5000
Fibre diameter	[µm]	14	50
Focal length collimator	[mm]	70	80
Focal length optics	[mm]	163	163
Focal diameter (measured)	[µm]	34	117

Table 3
Material properties of Al99.5, Cu-ETP and CuSn6 (Hummel et al., 2020; DKI Deutsches Kupferinstitut, 2005a, 2005b; Wieland SMH, 2018; Sicius, 2021).

Material Property (T = 20 °C)	Unit	Al99.5	Cu-ETP	CuSn6
Density	[g/cm^3]	2.7	8.9	8.8
Absorption (λ ≈ 1 µm)	[%]	≈ 9	≈ 5	≈ 10
Melting point	[°C]	660	1083	1050
Evaporation Temperature	[°C]	2470 (Al)	2595 (Cu)	2595 (Cu)
Electrical conductivity	[MS/m]	34–36	57	9
Thermal conductivity	[W/m•K-1]	210–220	394	75
Coefficient of thermal expansion	[10–6•K-1]	24	17	19

in the aluminium reference, showing material intermixing with the denser copper material. These visible process characteristics are then used to derive explanatory approaches and solution strategies.

3. Results and discussion

In the following the results of the experimental study are shown and analysed. The investigation is focused on pore formation and movement as well as on the intermixing of the materials.

3.1. Analysis of pore formation and movement

3.1.1. Aluminium on copper welds

The formation of pores is a usual defect for aluminium and copper welds. Using synchrotron radiation, the point of origin as well as the movement of the pores within the melt pool can be analysed.

From the investigations three main locations for pore formation depending on the welding configuration are identified:

1. Formation of pores in front of the keyhole at the material transition layer of aluminium-to-copper-welds.
2. The solidification area in aluminium while welding aluminium on copper connections.
3. The keyhole ground when welding copper on aluminium.

The first phenomenon is presented in Fig. 3. In front of the keyhole, a semi-circular bubble is formed, see marked circle. In the image sequence the bubble is growing. The movement and solidification of the bubble cannot be seen due to the lack of visibility in the copper material. A possible reason is an uprising movement along the keyhole due to the rising metal vapour. It can be assumed that the material transition is an obstacle for vapour and melt pool flows due to different physical properties of the materials.

Another possible reason for the formation of the pores is the different melting temperature of the two materials. Due to the higher melting point of copper and the higher energy content in the melt, the aluminium melt can overheat locally on contact layer and thus promote the formation of pores.

Increasing the focal diameter in the same configuration leads to an elongation of the melt pool in aluminium. More significant melt pool waves can be recognized on the surface in Fig. 4. The single images are showing different welding parameters with the same focal diameter. In the left image the significant number of bubbles in the solidification area is noticeable. Reviewing the full video sequence, the bubbles float back and forth, while bubbles are rising from the copper. The melt pool in copper is presumably shorter than in the aluminium. Therefore, the vertical flows disappear in the solidification area of the aluminium. Most of the bubbles can't reach the material surface and resume in the solidified weld seam as pores.

By increasing laser power and feed rate, this phenomenon cannot be detected, see Fig. 4 right. For a further investigation in this configuration, a view into the copper is necessary for a detailed discussion of the influence of the spot diameter. At present, differences in the width of the vapor capillary and the melt pool length can be identified. Pore formation can occur with both beam diameters.

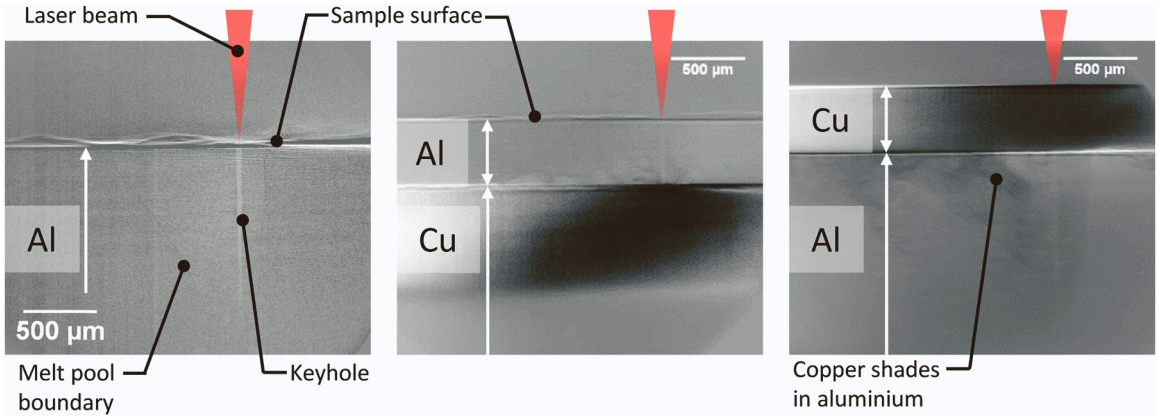

Fig. 2. Synchrotron images of the configurations (left: Al99.5 bead on plate, centre: Al99.5 to CuSn6, right: Cu-ETP to Al99.5).

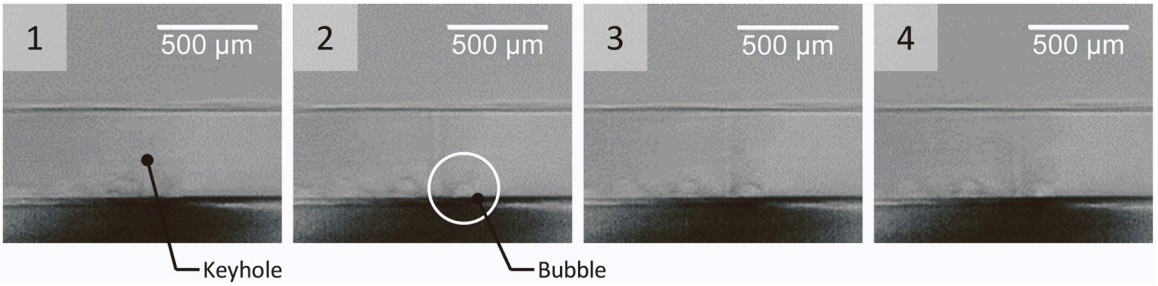

Fig. 3. Bubble formation in front of the keyhole - aluminium on copper ($P_L = 750$ W, $v_f = 50$ mm/s, $d_f = 34$ µm, $\Delta t = 1$ ms, related video sequence online available: https://doi.org/10.5281/zenodo.6411749).

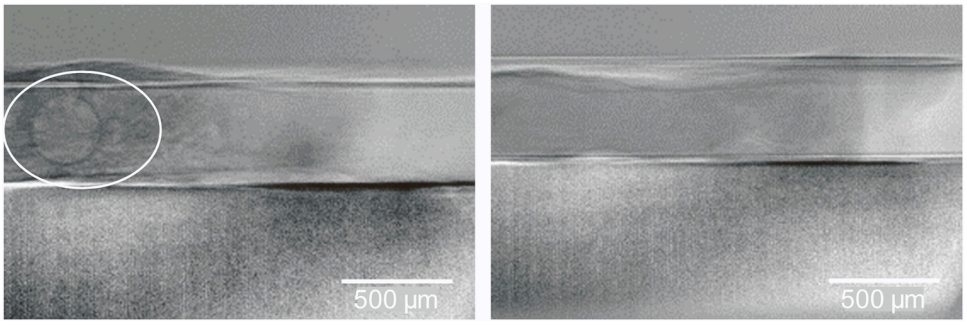

Fig. 4. Floating bubbles in the aluminium melt pool – aluminium on copper (df = 117 µm; left: P_L =1000 W, $v_f = 50$ mm/s; right: $P_L = 1500$ W, $v_f = 100$ mm/s).

3.1.2. *Copper on aluminium welds*

When changing the top material from aluminium to copper, the pore formation and movement in the melt pool ground becomes visible, see Fig. 5. The bubbles occur in the keyhole ground and are moving along the melt pool ground (B). Due to the lower thermal conductivity, the copper melt pool on top is smaller than the aluminium melt pool below. The bubbles, moving along the solidification line, are trapped in the material transition and solidify as pores (A). Some of them detach from the keyhole ground and directly rise to the material transition (C). Both motion paths show two distinct flow fields within the melt pool (metal vapour induced flow and capillary flow) (Beck, 1996).

The cross-section of the weld seam confirms the effect, see Fig. 6. The number of pores in the lower aluminium material is significantly higher than in copper. In the transverse cross-section one of the pores is trapped directly under the unmolten copper material. The longitudinal cross-section indicates pores along the whole depth of the weld seam.

The intermixing of the materials can also have an influence of the bubble movement and prevents their rising to the surface. In Fig. 7, the movement of a pore is marked in an image sequence. The last image summarizes the movement path on one specific bubble indicated with the number of the images and the resulting path geometry. In the images 4–6 dark shades (e.g. copper melt) are influencing the bubble movement. The movement direction is changed, and the upward movement prevented.

Additionally, it can be assumed that there is a movement in the image plane, vertically to the feed direction in frame 4–6. Due to the narrower copper melt pool, the copper shades are penetrating centrally into the aluminium. The forward copper flow pushes the bubble to the melt pool sidewall where it solidifies as a pore. This hypothesis is supported by the metallographic analysis in Fig. 8 which shows pore formation at the upper part of the lower joining partner at the outside of the weld seam.

The presented experimental results require a further investigation to outline the influence of the laser spot diameter and process parameters on the pore formation as well as a visibility with the given observation method inside the copper material.

3.2. *Analysis of melt pool dynamics*

The intermixing of the materials is a major concern during the welding of aluminium and copper due to the formation of intermetallic phases. In the following, the movement and mixing of the copper in the aluminium melt pool is analysed. Using synchrotron radiation, new opportunities in the analysis are available compared to conventional

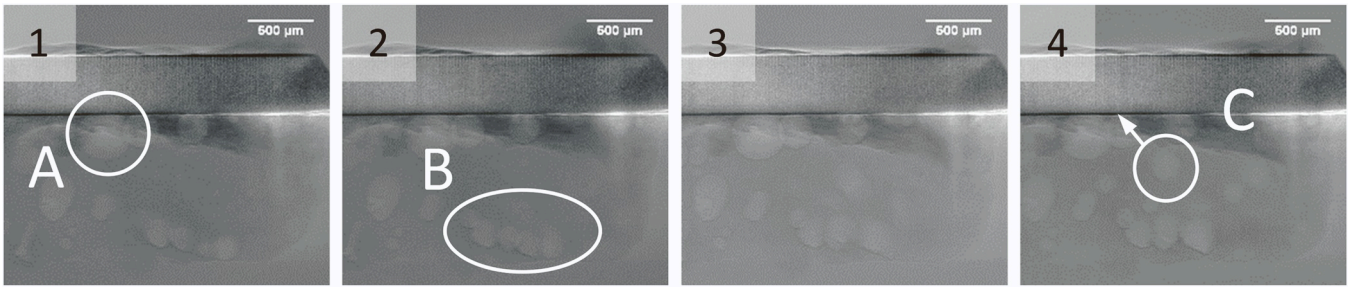

Fig. 5. Pore formation and movement in the melt pool ground – copper on aluminium ($P_L = 1000$ W, $v_f = 50$ mm/s, $d_f = 117$ µm, $\Delta t = 2$ ms, related video sequence online available: https://doi.org/10.5281/zenodo.6411749).

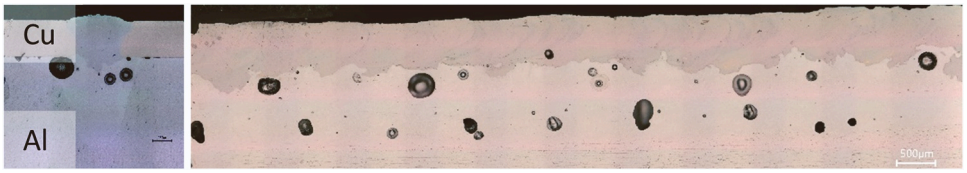

Fig. 6. Transverse and longitudinal cross-section of the weld seam – copper on aluminium.

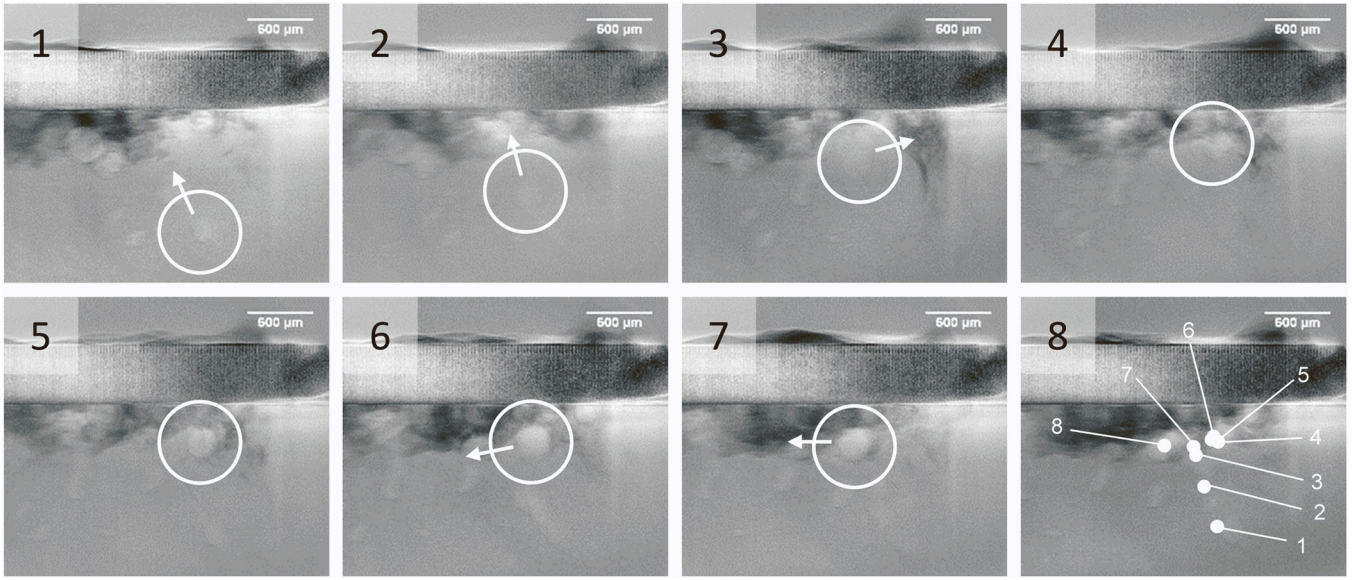

Fig. 7. Bubble movement influenced by material intermixing – copper on aluminium ($P_L = 1500$ W, $v_f = 100$ mm/s, $d_f = 117$ µm, $\Delta t = 2$ ms, related video sequence online available: https://doi.org/10.5281/zenodo.6411749).

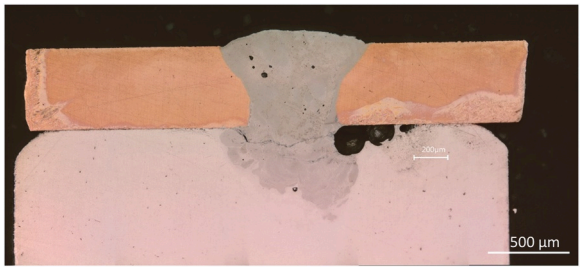

Fig. 8. Transverse cross-section to confirm the appearance of pores at the outside of the weld seam – copper on aluminium.

metallographic analysis. The image sequences analysed in this investigation are showing a batchwise flow of copper from the backside of the melt pool, see Fig. 9. The material is flowing towards the keyhole, where it is entrained by the capillary flow and swirled into the aluminium. The copper is mixed along the whole depth of the weld seam.

The same phenomenon is visible in the experiments with the smaller spot diameter. Using the parameters mentioned in Fig. 10, the copper shades are moving towards the keyhole and are pushed to the melt pool ground while intermixing with the aluminium.

Depending on the laser beam diameter, the images are showing a significant difference in the appearance of bubbles. While the welding process with $d_f = 117$ µm, shown in Fig. 5, Fig. 7 and Fig. 9, lead to bubbles, the welding process with $d_f = 34$ µm has no visible bubble in the presented sequence in Fig. 10.

The welding parameters have a strong influence on the intermixing of the materials. In Fig. 11, single frames of four different parameter sets are presented. Frames 1 and 2 differ in the feed rate. While the copper in 1 is mixed along the whole depth, the copper flow with increased feed rate is much smaller and closer to the material transition. It is to be mentioned, that the increase of the feed rate leads to a reduction of the weld depth. The marked weld depth is determined by analysing the full video due to the challenging visibility in a single frame.

Images 3 and 4 are welded using a circular spatial power modulation. Again, the mixing appearance is different compared to frames 1 and 2. The higher frequency of the oscillation leads to a more homogeneous mixing of the materials in frame 4. Both comparisons allow the assumption that due to the higher movement speed of the laser beam on the material surface and thus of the keyhole in the melt, the flow vectors are more strongly aligned in the horizontal direction and thus less mixing of the materials can take place in the vertical direction. On the other hand, more bubbles along the material transition are visible as well. Especially for the high dynamic spatial power modulation a higher frame rate needs to be achieved for the synchrotron analysis to capture every position of the keyhole inside the melt pool. Typical oscillation frequencies up to 1000 Hz are not covered with the actual set up but are subject to further investigations.

3.3. Discussion of the melt pool movement in aluminium and copper welding

Based on the results, a schematic illustration of the melt flow for aluminium and copper welds can be created, see Fig. 12.

During evaporation in the keyhole, the metal vapor rises and causes an upward melt flow along the capillary wall. A backward flow of material occurs due to the movement of the keyhole through the metal. It can be assumed that the combination of flow mechanisms creates a backward vortex in the copper. The copper is entering the aluminium at the end of the copper melt pool. Due to the wavy melt pool surface

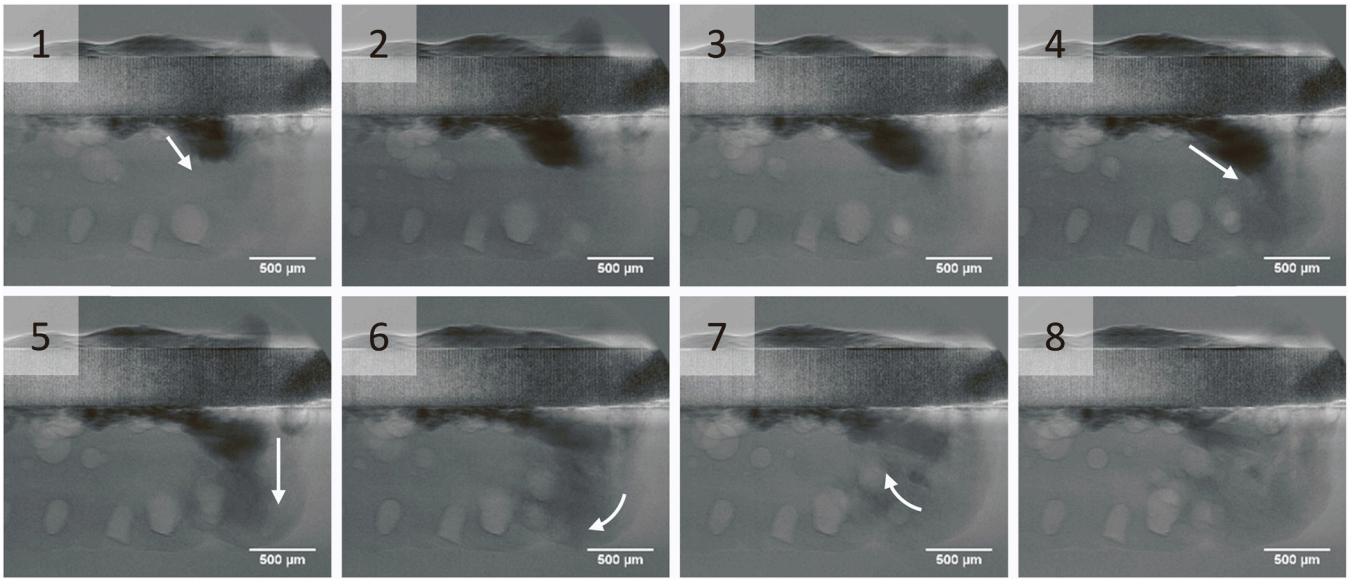

Fig. 9. Copper flow towards the keyhole – copper on aluminium (P_L = 1000 W, v_f = 50 mm/s, d_f = 117 µm, Δt = 1 ms, related video sequence online available: https://doi.org/10.5281/zenodo.6411749).

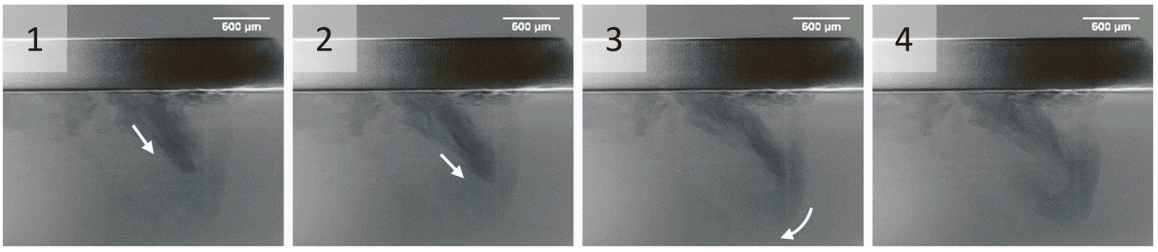

Fig. 10. Copper flow with smaller laser spot diameter – copper on aluminium (P_L = 750 W, v_f = 50 mm/s, d_f = 34 µm, Δt = 1 ms, related video sequence online available: https://doi.org/10.5281/zenodo.6411749).

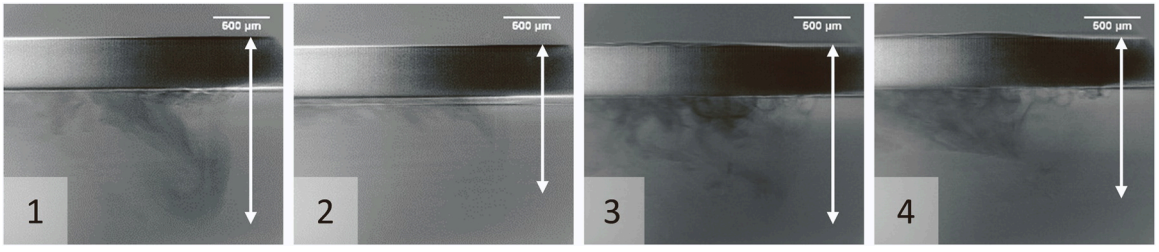

Fig. 11. Parameter-dependent copper flow (1 (Basic parameters): P_L = 750 W, v_f = 50 mm/s, d_f = 34 µm, 2: v_f = 100 mm/s, 3: A_s = 0,2 mm, f_s = 250 Hz, 3: A_s = 0,2 mm, f_s = 500 Hz).

characteristic the batchwise copper flow is induced. The higher density of copper supports the penetration of the copper melt into the aluminium. (Leitz, 2016) explained the vertical backward flow with the evaporation pressure that accelerates the melt in front of the keyhole. By reaching the keyhole, the copper shade is accelerated to the melt pool ground and moves along the solidification border to the back of the melt pool. Comparable to the bubble movement the copper flow is deflected at the material transition due to the smaller copper melt pool. A mixing along the whole depth is visible.

The illustrated melt flows are approaches for an explanation of the material mixing. The high dynamics of the flows in the melt pool lead to complex flow situations, which are shown in simplified form in Fig. 12. For the confirmation of the hypotheses, further investigations with higher temporal resolution of the imaging method are necessary. Especially the influence of different parameters, as indicated by doubling the feed rate in Fig. 11, has a major influence on the melt flow. With regard to a comparison of the two beam diameters, it can be stated that the batchwise penetration of the copper melt in the direction of the keyhole occurs in both cases but differs in terms of the intensity and size of the copper stream. To gain further information about the melt flow, the visibility of the copper melt pool in the x-ray analysis should also be achieved in further investigations.

4. Conclusion

In conclusion, it was shown that high energy synchrotron radiation is able to give an insight into the welding process of aluminium and copper. The approach can help to understand the melting and mixing

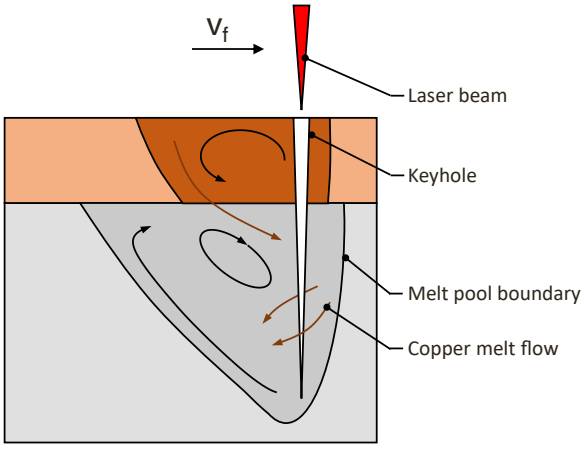

Fig. 12. Schematic illustration of the melt pool flows.

behaviour of the materials as well as the pore formation considering the different parameters applied. The following observations can be derived from this work:

- The different material properties and thus different melt pool extensions in dissimilar material joints cause a difference in the melt pool length of copper and aluminium. The uprising bubbles are trapped at the material transition area and remain as pores in the joint.
- Regarding the intermixing of the materials a batchwise penetration of the copper into the aluminium could be observed in the copper and aluminium joint.
- Changing the welding parameters, such as laser power, feed rate, spot diameter or spatial power modulation, can lead to a massive change of the melt flows and intermixing. In the parameter range used, an increase in the feed rate leads to a reduced penetration depth of the copper into the aluminium below.
- The observed penetration of the copper into the aluminium occurs with both beam diameters used. The number and size of pores might be lower with the smaller spot diameter when aluminium is the bottom material.

To reduce the appearance of intermetallic phases in these dissimilar joints, the influence of the parameters can be investigated in future experiments. Upcoming studies will investigate the influence on reducing the intermetallic phases by adapting process parameters according to the results of the x-ray observation. To increase the precision of the presented analyzation method, future improvements must deal with the frame rate and the visibility of melt pool in copper. This allows differences between the two material arrangements to be analysed. The increasing understanding of the formation of pores and intermetallic phases enables the development of specific compensation methods such as beam shaping, temporal or spatial power modulation. A deep process knowledge is the basis for the industrial use of aluminium and copper connections in electromobility.

CRediT authorship contribution statement

S. Hollatz: Conceptualization, Methodology, Validation, Investigation, Writing – original draft. **M. Hummel:** Conceptualization, Methodology, Investigation, Writing – review & editing. **A. Olowinsky:** Conceptualization, Methodology, Investigation, Writing – review & editing. **A. Gillner:** Conceptualization, Supervision, Project administration, Funding acquisition. **F. Beckmann:** Methodology, Investigation. **J. Moosmann:** Methodology, Investigation.

Declaration of Competing Interest

The authors declare the following financial interests/personal relationships which may be considered as potential competing interests: Marc Hummel reports equipment, drugs, or supplies was provided by IPG Photonics Corp. Marc Hummel reports equipment, drugs, or supplies was provided by TRUMPF Laser GmbH.

Data Availability

Links to high speed videos are included in the paper.

Acknowledgements

The presented investigations were carried out at RWTH Aachen University within the framework of the Collaborative Research Centre SFB1120–236616214 “Bauteilpräzision durch Beherrschung von Schmelze und Erstarrung in Produktionsprozessen” and funded by the Deutsche Forschungsgemeinschaft e.V. (DFG, German Research Foundation). The sponsorship and support are gratefully acknowledged.

This research was supported by TRUMPF GmbH & Co. KG and IPG Laser GmbH. We would like to thank all people involved for their support. The presented investigations were carried out in cooperation with DESY in Hamburg at PETRA III and we would like to thank F. Beckmann and J. Moosmann for assistance in using P07 EH4.

References

Balu, Prabu; Carlson, Blair; Kovacevic, Radovan (2011): An Investigation into the Laser Micro-Welding of Aluminum and Copper in Lap Joint Configuration. In TMS annual Meeting (Vol. 3), pp. 295–307. doi: 10.1002/9781118062173.ch37.

Bantel, C., 2018. Laserstrahlschweißen von Aluminium-Kupfer-Verbindungen. Dissertation: Technische Universität Dresden.

Beck, Markus, 1996. Modellierung des Lasertiefschweißens. Teubner (Laser in der Materialbearbeitung Forschungsberichte des IFSW), Zugl.: Stuttgart, Univ., Diss. Stuttgart.

Brand, Martin J., Schmidt, Philipp, A., Zaeh, Michael, F., Jossen, Andreas, 2015. Welding techniques for battery cells and resulting electrical contact resistances. J. Energy Storage 1, 7–14. https://doi.org/10.1016/j.est.2015.04.001.

Cunningham, R., Zhao, C., Parab, N., Kantzos, C., Pauza, J., Fezzaa, K., Rollett, A.D., 2019. Keyhole threshold and morphology in laser melting revealed by ultrahigh-speed x-ray imaging. Science 363 (6429), 849–852. https://doi.org/10.1126/science.aav4687.

Das, Abhishek, Li, Dezhi, Williams, David, Greenwood, David, 2018. Joining technologies for automotive battery systems manufacturing. WEVJ 9 (2), 22. https://doi.org/10.3390/wevj9020022.

Dimatteo, Vincenzo, Ascari, Alessandro, Fortunato, Alessandro, 2019. Continuous laser welding with spatial beam oscillation of dissimilar thin sheet materials (Al-Cu and Cu-Al): process optimization and characterization. J. Manuf. Process. 44, 158–165. https://doi.org/10.1016/j.jmapro.2019.06.002.

DKI Deutsches Kupferinstitut (2005a): Werkstoff-Datenblatt: Cu-ETP. Available online at ⟨https://www.kupferinstitut.de/wp-content/uploads/2019/11/Cu-ETP.pdf⟩, checked on 7/23/2021.

DKI Deutsches Kupferinstitut (2005b): Werkstoff-Datenblatt: CuSn6. Available online at ⟨https://www.kupferinstitut.de/wp-content/uploads/2019/11/CuSn6–1.pdf⟩, checked on 2/14/2022.

Fetzer, F.; Berger, P.; Hu, H.; Weber, R.; Graf, T. (2018): Pores in laser beam welding: generation mechanism and impact on the melt flow. In Proc. SPIE 10525, High-Power Laser Materials Processing: Applications, Diagnostics, and Systems VII 105250D. doi: 10.1117/12.2295798.

Hügel, Helmut, Graf, Thomas, 2009. Laser in der Fertigung, Vol. 2. Vieweg+ Teubner, Wiesbaden.

Hummel, Marc, Schöler, Christoph, Häusler, André, Gillner, Arnold, Poprawe, Reinhart, 2020. New approaches on laser micro welding of copper by using a laser beam source with a wavelength of 450 nm. J. Adv. Join. Process. 1 (100012) https://doi.org/10.1016/j.jajp.2020.100012.

Hummel, Marc Daniel; Halm, Ulrich; Hagenlocher, Christian; Lind, Jannik; Hollatz, S.ö ren; Häusler, André et al. (2021): Temporally and spatially highly resolved reconstruction of vapor capillary geometry during laser beam welding using synchrotron radiation. Edited by Lasers in Manufacturing Conference 2021. München (RWTH-2021–05994). Available online at ⟨https://publications.rwth-aachen.de/record/821069⟩.

Kalman, R.E., 1960. A new approach to linear filtering and prediction problems. J. Basic Eng. 82 (1), 35–45. https://doi.org/10.1115/1.3662552.

Kraetzsch, M., Standfuss, J., Klotzbach, A., Kaspar, J., Brenner, B., Beyer, E., 2011. Laser beam welding with high-frequency beam oscillation: welding of dissimilar materials

with brilliant fiber lasers. Phys. Procedia 12, 142–149. https://doi.org/10.1016/j.phpro.2011.03.018.

Lee, S.Shawn; Kim, Tae H.; Hu, S.Jack; Cai, Wayne W.; Abell, Jeffrey A. (2010): Joining Technologies for Automotive Lithium-Ion Battery Manufacturing: A Review. In *Proceedings of the ASME 2010 International Manufacturing Science and Engineering Conference*, pp. 541–549. doi: 10.1115/MSEC2010–34168.

Leitz, Andreas (2016): Laserstrahlschweißen von Kupfer- und Aluminiumwerkstoffen in Mischverbindung. Dissertation, Universität Stuttgart. München: Herbert Utz Verlag (Laser in der Materialbearbeitung - Forschungsberichte des IFSW).

Miyagi, Masanori, Kawahito, Yousuke, Kawakami, Hiroshi, Shoubu, Takahisa, 2017. Dynamics of solid-liquid interface and porosity formation determined through x-ray phase-contrast in laser welding of pure Al. J. Mater. Process. Technol. 250, 9–15. https://doi.org/10.1016/j.jmatprotec.2017.06.033.

Rabkin, D.M., Ryabov, V.R., Lozovskaya, A.V., Dovzhenko, V.A., 1970. Preparation and properties of copper-aluminum intermetallic compounds. Powder Met. Met. Ceram. 9, 695–700. https://doi.org/10.1007/BF00803820.

Schell, Norbert; King, Andrew; Beckmann, Felix; Fischer, Torben; Müller, Martin; Schreyer, Andreas (2013): The High Energy Materials Science Beamline (HEMS) at PETRA III. In Mechanical Stress Evaluation by Neutrons and Synchrotron Radiation VI 772, pp. 57–61. doi: 10.4028/www.scientific.net/MSF.772.57.

Schmidt, Philipp A.; Schweier, Markus; Zaeh, Micheal F. (2012): Joining of lithium-ion batteries using laser beam welding: Electrical losses of welded aluminum and copper joints. In ICALEO 2012, pp. 915–923. doi: 10.2351/1.5062563.

Schmitt, F., 2012. Laserstrahl-Mikroschweißen mit Strahlquellen hoher Brillanz und örtlicher Leistungsmodulation. Dissertation. RWTH Aachen University. Aachen: Shaker.

Sicius, Hermann, 2021. Handbuch der chemischen Elemente. Springer Berlin Heidelberg, Berlin, Heidelberg.

Wagner, Jonas, Hagenlocher, Christian, Hummel, Marc, Olowinsky, Alexander, Weber, Rudolf, Graf, Thomas, 2021. Synchrotron X-ray analysis of the influence of the magnesium content on the absorptance during full-penetration laser welding of aluminum. Metals 11 (5), 797. https://doi.org/10.3390/met11050797.

Wieland SMH (2018): Werkstoff-Datenblatt: EN AW-1050A. Available online at ⟨https://www.wieland-smh.de/files/smh/wieland_smh/dat%20sheets/EN-AW-1050A_DE.pdf⟩, checked on 7/23/2021.

Xu, J., Rong, Y., Huang, Y., Wang, P., Wang, C., 2018. Keyhole-induced porosity formation during laser welding. J. Mater. Process. Technol. 252, 720–727.

Zhao, C., Parab, N.D., Li, X., Fezzaa, K., Tan, W., Rollett, A.D., Sun, T., 2020. Critical instability at moving keyhole tip generates porosity in laser melting. Science 370 (6520), 1080–1086. https://doi.org/10.1126/science.abd1587.